Depositional characteristics and special distribution of deep-water sedimentary systems on the northwestern middle-lower slope of the Northwest Sub-Basin, South China Sea

Hui Chen [1, 2], Xinong Xie [1, ✉], David Van Rooij [2], Thomas Vandorpe [2], Li Huang [1], Laiyuan Guo [1], Ming Su [3, 4]

(1) Key Laboratory of Tectonics and Petroleum Resources of Ministry of Education, Faculty of Resources, China University of Geosciences (Wuhan), 430074 Wuhan, China

(2) Ghent University, Department of Geology and Soil Science, Renard Centre of Marine Geology, Krijgslaan 281 s8, B-9000 Ghent, Belgium

(3) Key Laboratory of Renewable Energy and Gas Hydrate, Guangzhou Institute of Energy Conversion, Chinese Academy of Sciences, 510640 Guangzhou, China

(4) Guangzhou Center for Gas Hydrate Research, Chinese Academy of Sciences, 510640 Guangzhou, China

✉ **Xinong Xie**

Key Laboratory of Tectonics and Petroleum Resources of Ministry of Education, Faculty of Resources, China University of Geosciences (Wuhan), 430074 Wuhan, China

E-mail: xnxie@cug.edu.cn; xnxie05@163.com

Tel: (+86) 27-6788 3653; Fax: (+86) 27-6788 3051.

Submitted to Marine Geophysics Research, special issue for the South China Sea

July, 23, 2013

Abstract

Based upon 2D seismic data, this study confirms the presence of a complex deep-water sedimentary system within the Plio-Quaternary strata on the northwestern lower slope of the Northwestern Sub-Basin, South China Sea. It consists of submarine canyons, mass-wasting deposits, contourite channels and sheeted drifts. Alongslope aligned erosive features are observed on the eastern upper gentle slopes (< 1.2° above 1500 m), where a V-shaped downslope canyon presents an apparent ENE migration, indicating a related bottom current within the eastward South China Sea Intermediate Water Circulation. Contourite sheeted drifts are also generated on the eastern gentle slopes (~1.5° in average), below 2500 m water depth though, referring to a wide unfocused bottom current, which might be related to the South China Sea Deep Water Circulation. Mass wasting deposits (predominantly slides and slumps) and submarine canyons are developed on steeper slopes (> 2°), where weaker alongslope currents are probably dominated by downslope depositional processes on these unstable slopes. The NNW-SSE oriented slope morphology changes from a three-stepped terraced outline (I-II-III) east of the investigated area, into a two-stepped terraced (I-II) outline in the middle, and into a unitary steep slope (III) in the west, which is consistent with the slope steepening towards the west. Such morphological changes may have possibly led to a westwards simplification of composite deep-water sedimentary systems, from a depositional complex of contourite erosive/depositional systems, mass-wasting deposits and canyons, on the one hand, to only sliding and canyon depositions on the other hand.

Keywords deep-water sedimentation · bottom current · contourite · mass-wasting deposits · South China Sea

1. Introduction

Deep-water sedimentary systems have been receiving intensive attention from the scientific community during the recent decades, due to their crucial importance for natural resources (e.g., deep-sea mineral deposits and hydrocarbon reservoirs) and for academic research (e.g., palaeoceanography and palaeoclimatology) (Mulder et al. 2011). The dynamic processes driven by downslope and alongslope currents play a significant role in the construction and shaping of continental margins (Stow et al. 2008; Mulder 2011). Through erosion, transport and deposition of sediments, these dynamic processes can generate a complex of deep-water sedimentary systems, including turbidite depositional systems, mass-wasting depositional systems and contourite depositional systems (Bouma 1964; Faugères and Mulder 2011; Hernández-Molina et al. 2011a). Under specific accumulation and preservation conditions, these deep-water sedimentary systems can record a wealth of information on palaeoceanographic changes, either in the sedimentary (small-scale) or geophysical (large-scale) record (Hernández-Molina et al. 2010; Frigola et al. 2008; Mulder et al. 2008).

The northwestern lower slope of the Northwest Sub-Basin from the South China Sea (SCS) represents a critical location in the SCS deep-water sedimentary dynamics, due to the convergence of the Xi'sha Trough, the SCS northwestern continental-oceanic transition zone and the abyssal plain (Fig. 1A). Deep-water downslope sedimentary systems have been widely studied in the SCS northern marginal basins, for instance, the Qiongdongnan Basin and Pearl River Mouth Basin (Liu et al. 2009 and references therein), and alongslope sedimentary systems have been reported on the southern slopes of the Dongsha Uplifts and the Taiwan Island (Shao et al. 2007; Wang et al. 2010; Gong et al. 2012). However, deep-water sedimentary systems on the oceanic-continental transition zone, which connects the Northwest Sub-Basin to the Xi'sha Trough, have been only tentatively described and analyzed in previous studies (Zhu et al. 2010; Li et al. 2013; Zheng and Yan 2012).

The main goal of this study is to unravel the margin architecture constructed by the different deep-water sedimentary dynamics in the northern SCS. This paper identifies and reports the Pliocene-Quaternary depositional characteristics and patterns of composite alongslope and downslope deep-water systems on the northwestern lower slope of the Northwest Sub-Basin of the SCS, located in water depths from ~1000 to ~3500 m (Fig. 2). An accurate description will be presented on (a) their spatial distribution, (b) the associated morphological features and (c) the internal structures of erosional and depositional processes, in association with gravity flow and bottom current activities. These observations may provide new insights in the SCS deep-water sedimentary systems as well as in the present-day governing oceanography.

2. Regional setting

2.1. Geological background

The SCS basin is a rhomb-shaped (southwest tapering) semi-closed basin and encompasses an area of about 3.5×10^6 km², which consists of three sub-basins (Northwest, Central/East and Southwest, Fig. 1) (Sun et al. 2009; Wang and Li 2009a). The study area is located on the northwestern margin of the SCS Northwest Sub-Basin (113°15’ E to 114°30’ E, 18° N to 19° N), in water depths between ~1000 to ~3500 m (Fig. 2). Additionally, it belongs to the southern uplift zone on the southwestern margin of the Pearl River Mouth Basin, which is a Cenozoic rift basin occupying an area of about 17.5×10^4 km^2 (Li et al. 2009). The local bathymetric map of the study area (Fig. 2) shows the presence of an alongslope aligned seamount, seated in the south of the Shenhu Area. Hence, it is proposed to name this the South Shenhu Seamount (SSS) after its locality. The study area is located northwest of the SSS.

This region experienced the initial spreading process of the SCS (32 to 30 Ma), which locally ended at 23

Ma (Sun et al. 2006). With the transformation of the northern SCS from a neritic continental shelf to a continental slope at the end of Oligocene (23 Ma) (Chen et al. 1993; Li et al. 2009), the deep-water sedimentation in the Pearl River Mouth Basin started since the Early Miocene (Shao et al. 2004; Xie et al. 2011). The main rivers, transporting sediments to the abyssal part of the northern SCS, are the Red River (Vietnam), the Pearl River (South China), the Central Canyon (the Qiongdongnan Basin, see the submarine canyon with yellow star shown on Fig. 1A, which is connected with the Xi'sha Trough) as well as rivers in southern Taiwan and in Luzon/Philippines (Liu et al. 2009 and references therein). They control the sediment supply to the basins and as a consequence the load of turbidity flows in this region.

The geophysical and borehole data related to ODP Sites 1146 and 1148 (Lüdmann et al. 2001; Wang et al. 2000) (Fig. 1B) enable to recognize three major breakup unconformities with ages of 5.2 Ma, 11.5 Ma and 23 Ma, named as T3, T4 and T6 respectively in the stratigraphic classification scheme proposed by Xie et al. (2011). Unconformity boundaries of T4 and T6 were recognized using seismic and well data from the industrial drilling of Well 1, which contains the available well data closest to the study area (see W1 on Fig. 1 for its location).

2.2. Oceanographic framework

ODP geophysical and borehole data show that the thermo-haline circulation within the SCS was relatively stable and sustainable from the Middle Miocene to Pliocene (Zhao 2005; Wang 2007). Li et al. (2008) investigated the deep water ventilation and stratification in the Neogene SCS, using combined data of physical properties, benthic foraminifera and stable isotopes from ODP Sites 1143, 1146 and 1148. They found that (1) the SCS deep water mass was freely connected to open ocean deep circulations before 10 Ma, but got gradually blocked due to the closure of the SCS basin from 10 Ma to 5 Ma, (2) from 5 Ma to 3 Ma the local SCS deepwater became strongly stratified, possibly due to a strengthening of the Pacific Deep Water, together with a global cooling event and a sea basin subduction, (3) From 3 Ma onwards, the SCS deep water evolved into its modern phase, with the nowadays mode starting to form at ~1 Ma, accompanied with the rise of sills under the Bashi Strait and the mid-Pleistocene climate transformer event.

The present-day SCS oceanic circulation is roughly divided into 3 vertical layers: the SCS surface water circulation (SSWC) (< 350 m), the SCS intermediate water circulation (SIWC) (~350 to at least 1350 m) and the SCS deep water circulation (SDWC) (> 1350 m) (Chen and Wang 1998; Zhu et al. 2010). The SSWC seasonally varies (cyclonic in winter and anti-cyclonic in summer) due to the bi-annual monsoon changes (Fang et al. 1998; Xue et al. 2004). Compared to the upper waters, the mid- and deep-water oceanography is much less studied (Wang and Li 2009b; Lüdmann et al. 2005; Tian and Qu 2012), whereas the occurring depths for the SIWC and SDWC are still in debate, e.g., newly published data indicate that the main scope of SIWC can easily access a water depth deeper than 1500 m (Wang et al. 2013; Xie et al. 2013). Published data show that SIWC is anti-cyclonic, and is commonly referred to as the Kuroshio Current and may locally contain the SCS warm current (Zhu et al. 2010; Yuan 2002; Chen 2005), while the SDWC is cyclonic (Wang et al. 2010; Shao et al. 2007) (Fig. 1). The SDWC is influenced by the intrusion of the southward flowing Northern Pacific Deep Water crossing the Bashi Channel (the average current velocity over the Bashi Channel exceeds 0.15 m/s and the maximum velocity of 0.3 m/s is reached at water depths of 2500 to 2600 m) (Xie 2009; Qu et al. 2006; Lüdmann et al. 2005; Gong et al. 2012) (Fig. 1A).

The SCS water circulation presents a vertical sandwich structure in the Luzon Strait, with surface (winter) and deeper waters flowing into the SCS from the Pacific and returning at upper (summer) and intermediate depths (Wang and Li 2009b; Yuan 2002; Qu and Lindstrom 2004).

3. Material and methods

For the aims of this study, a data set of over 1500 km multichannel 2D airgun reflection seismic profiles covering an area of > 4200 km² was analysed, provided by the Nanhai West Oil Corporation, a division of China National Offshore Oil Corporation (CNOOC). The seismic profiles are oriented NNW-SSE and ENE-WSW, with spacing of about 3-6 km and 2-8 km in average, respectively. In order to quantify seabed morphologies, the vertical scale of these profiles was converted from two-way travel time to depth using a P-wave velocity of 1500 m/s for the water column.

The seismic signals were obtained using a Bolt Longlife Airgun with a volume of 3850 cubic inches, generated by means of compressed air (2000 psi). The record length was set to 11996 ms TWT with a sampling rate of 2 ms. The acquired signals were recorded within 396 channels using a fold of 99, and lie in the frequency range of about 60 Hz, allowing a vertical resolution of up to 3 m. The data was processed by CNOOC, using Omega V1.8.1 software and applying (1) a bandpass filter ranging from 6 Hz (low-cut frequency), 12 dB/s (low-cut slope) to 136 Hz (high-cut frequency), 276 dB/s (high-cut slope), (2) A de-noising and amplitude compensations and (3) a post-stack time migration (Kirchhoff). After being processed, the seismic data were loaded into a Kingdom Suite (V8.3, 32-bit) project (UTM projection, zone 49) for horizon picking and sediment dynamic interpretations.

4. Results

On the topographic map of the investigated area (Fig. 2), the WSW-ENE oriented SSS in the northwest and the W-E oriented Xi’sha Trough in the southwest can be observed as remarkable morphologic features. Series of downslope submarine canyons are observed developing on slopes lower than 1500 m in the northwest of the study area. Slopes of the investigated margin decline to the southeast, where the SCS abyssal plain reaches more than 3500 m in depth. In the NNE-SSW direction, the slope morphology in the eastern part of the study area presents a terraced outline (Figs. 3 and 4). Roughly, the upper (< 1500 m) and lower (> 2500 m) parts (I and III) are gentle slopes (< 1.5°) while the middle part (II) is steeper (> 2°). This terraced slope morphology is not apparent on Figs. 5 and 6, and gradually loses its expression westwards (Fig. 7). Erosive and depositional structures, related to both alongslope and downslope currents, are observed on these investigated slopes, which will be described in detail in following sections.

The through-well (W1) seismic line (see its location on Fig. 1), which contains the 2D seismic profile of Fig. 3 as its southeastern section, helps establish the framework of closure seismo-stratigraphic interpretations covering the investigated area. Break-up unconformities of T4 (11.5 Ma) and T6 (23 Ma) can be recognized and traced over the study area, while the unconformity of T3 (5.2 Ma) is much less obvious (Figs. 3-8). Additional sedimentological data are required to exactly identify the unconformity T3, however, the depositional and erosive features that have been investigated in this study are surely constrained between T3 and the seafloor, within the Pliocene-Quaternary strata.

4.1. Submarine canyons and the Xi'sha Trough

The bathymetric map and reflection seismic profiles reveal that submarine canyons are widespread on the northwestern margin of the Northwest Sub-Basin in the SCS (see the yellow dashed lines in Fig. 2). The seismic profiles discussed in this paper cover eight submarine canyons (*C. 1* to *C. 6*, *C'* and *C''*), which are identified through a) their typical incision morphologies as well as b) the discontinuous-chaotic and high amplitude reflectors of sediments within the canyons (Figs. 3 to 8). The W-E oriented Xi'sha Trough runs along the southern margin of the study area and enters into the abyssal plain of the northern SCS (Figs. 1 and 2), which is covered by seismic profiles of Figs. 5, 6, 7 and 8B. Detailed information on these canyons and the Xi'sha

Trough (e.g., orientations, locations, dimensions and morphologies) is presented in table 1.

C. 1 has a NNW-SSE orientation above 2000 m in water depth and changes to a WNW-ESE orientation, below 3500 m water depth cutting the lower slopes and entering into the abyssal plain (Figs. 2, 3, 4 and 8A). On the gentle mid-upper slope (~1350 m in water depth and ~1° slope) of the study area, the NNW-SSE oriented *C. 1* shows an asymmetric V-shaped morphology (slopes of 2.2° for its WNW flank and 3.9° for the ENE), with ~140 m of incision and ~6.5 km in width (Figs. 2 and 8A). From the seismic profile of Fig. 8A, successive erosion bases within *C. 1* can be identified (see dashed lines in yellow in Fig. 8A), which show continuous, high amplitude seismic reflections, incising into underlying layers. The stacking pattern of these successive incisions shows an obvious migration toward ENE.

On the mid-slope of the study area, both *C. 2* and *C. 3* have the NNE-SSW orientations spanning from ~1900 to proceeding 2500 m in water depths (Figs. 2, 5 and 6). *C. 4* and *C. 6* are recognized developing on the lower over steepened slopes with water depth > 2500 m and slope > 5° (Figs. 2 and 9), which show limited lengths on the plane (< 5 km) (Fig. 2) but deep incisions (exceeding 200 m) (Table 1; Fig. 8b).

~15 km to the east of *C. 2*, *C. 5* cut the mid-slope of the study area from ~1400 to ~2500 m in water depths (Figs. 2 and 7). On the seismic profile of Fig. 8C (~1790 m in water depth and ~2° of slope), it shows a U-shaped morphology with a flat bottom, with a slightly mounded levee-system developed on both flanks of the canyon. The levee-system shows high amplitude and fairly continuous seismic reflection, developing a more or less aggradational pattern (Fig. 8C). Note that the levee sediments on the ENE side of *C. 5* show flat and parallel/sub-parallel reflectors, while on the WSW side continuous wave-shaped reflectors are presented. Additionally, two small scale canyons (C’ and C”) are recognized on the seismic profile of Fig. 7 (Table 1).

4.2. Mass-wasting deposits

Mass-wasting deposits are widely developed on a high-gradient slopes (> 2°), covering an area of about 600 km^2 and presenting parallel to sub-parallel, moderate to high amplitude seismic reflections (Figs. 3 to 7). Morphological features identified within those slope failure deposits include the headwall scarp, successive overlapped slumps, failure surfaces, slide scars and detached slumps.

The headwall scarp is termed as the upper part of where failure took place and downslope movement originated, vacated by the displaced mass (Varnes 1978; Hampton and Lee 1996). A headwall scarp with height of ~50 m is identified, as the head part of the mass-wasting area, at water depth of ~1500 m with slope > 2.35° on the seismic profile of Fig. 6.

The successive overlapped slumps, introduced by (Mulder and Cochonat 1996), are recognized in the upper section of mass-wasting area on > 2° slopes between ~1300 and ~1700 m in depths. They are characterized by that one slump body is merged with the failure surfaces of the following slumps, which are continuous from one edge of the slump to the other (Figs. 3, 4, 5 and 7).

Detached slumps are shown as step-forming detached sediment masses, giving a general staircase-like pattern (Laberg and Vorren 2000; Lastras et al. 2006). Their slightly curved steps are oriented perpendicular to the direction of mass-wasting motion, and are separated from each other by small slide scars (Figs. 3, 4 and 6). Major detached slumps are observed locating at the lower slopes in vicinity of successive overlapped slumps (water depth > 1500 m and slope > 2.35°), and compared with the later slumps they are more discontinuous and degraded. On the seismic profile of Fig. 6, detached slumps are also developed at water depths from ~1900 to ~2200 m, as the upper head section of the slide scar area with over steepened slopes (> 4.5°).

In the eastern part of the study area, mass-wasting deposits are restricted between ~1500 and ~2000 m water depth, with contourite erosive features developed on the upper continental slopes in the north, and sheeted drift deposits on the lower slops in the south (Figs. 3 to 5). From east to west the spatial distribution of mass-wasting deposits is expanding, and in the western part they cover the depth range from ~1450 to ~2100 m on Fig. 6 and from ~1250 to ~2250 m on Fig. 7.

4.3. Wavy sediments

Wavy sediments are not widely developed through the study area, only showing up within the mass-wasting area (Figs. 5, 7 and 8). More precisely, they are developed on slopes with water depths between ~1800 to ~2000 m and ~1.3° to ~2° of slope, where canyons of *C. 2*, *C. 5*, *C'* and *C"* are appeared in neighbourhood. These wavy sediments show fairly continuous and parallel, moderate to high amplitude seismic reflections, with the structure of internal reflectors similar from one wave to the next. The apparent boundaries between waves are typically linear or convex upwards and the sediment beds appear more continuous than other displaced mass deposits nearby. Waves presented on both seismic profiles of Figs. 5 and 7 show upslope migrations: 1) within the wavy sediments on the SSE side of *C. 2*, the waves have their downslope (SSE) flanks eroding sediments while the upslope (NNW) flanks accumulating, with ~2.25 km of wave length and ~55 m of wave height in average (Fig. 5); 2) the overall wave field (~0.75 km of wave length and ~10 m of wave height in average) between the upslope (NNW side) *C'* and the downslope (SSE side) *C"* has a concave-upward surface, while close to *C"* it seems developing a failure surface (Fig. 7); 3) waves on the upslope of *C'* have an average wave length of ~1.5 km and wave height of ~30 m (Fig. 7). Waves observed on the seismic profile of Fig. 8 are developed within the levee system of *C. 5* on its WSW flank, with ~1.9 km of wave length and ~20 m of wave height in average and following an aggradational pattern.

4.4. Contourite drifts, channels and moats

The contouritic sheeted drifts are spread out across continental margins where a gentle gradient and smooth topography favour a wide non-focused bottom current (Faugères et al. 1999; Faugères and Stow 2008). Sheeted drift deposits can be recognized draping relatively deep (> 2500 m) and gentle (~1.5°) slopes in the southeastern part of the study area, with an average thickness over 70 ms TWT (Figs. 3 to 5, 8b). On the seismic profiles, these deposits show fairly continuous, parallel to sub-parallel reflectors of moderate amplitudes. Their morphologies are mostly flat and smooth, except when (1) they become deformed in association with marginal faults (Figs. 3, 4, 5 and 9), and when (2) they are affected by submarine canyons (Figs. 3 to 5). From east to west, the development of sheeted drifts gradually reduces, which might be associated to the disappearance of the lower gentle shapes (Figs. 6 and 7).

Contourite channels are erosive features with a margin-parallel trend that are formed mainly by the erosive action of bottom currents, and furrows are termed for depressions with incisions < 10 m (Faugères et al. 1999; Hernández-Molina et al. 2006). Small scale alongslope aligned channels (~0.5 to ~2 km wide and ~10 to ~20 m deep) and furrows are present on the northeastern slopes (at water depths of ~1500 m and above where the slope is < 1.14°), on the NNE-SSW oriented 2D seismic profiles of Figs, 3 to 6. Some of these channels are developed within recent strata (Figs. 3, 5 and 6), while some of them show consistent signs of erosions (more or less aggradational) underlying, which can be tracked back to the early Late Miocene (after 11.5 Ma) (Fig. 4). Latest depositions can be observed infilling within these contourite channels, while the rest slopes nearby show non-deposition features (Figs. 3 to 6). Approximately 20 km west of Fig. 4, the SSS appears (Fig. 2). When following the contour line of ~1500 m to the west, we see that those erosion and non-deposition features gradually lose their expressions, where mass-wasting deposits are developed instead, on the slopes south of the SSS (slope of 2.07°) (Fig. 7).

Contourite moats differ from contourite channels in their genetic relation with mounded and elongated separated drifts (Faugères et al. 1999; Hernández-Molina et al. 2006). The typical nature of moats is missing on the investigated seismic profiles, but the bathymetric map shows a remarkable moat flanking the northern SSS

(Figs. 2). Depositional features and processes of bottom currents on the slopes north of the SSS are beyond the scope of this study, but will be introduced and discussed in (Chen et al. submitted).

With the slope morphology steepening from east (< 1.5°) to west (> 2°), the development of sheeted drifts stops when the gentle lower terrain (~1.5° of slope and > 2500 m in water depth) disappears, while contourite erosions and non-deposition features disappear near the SSS (Figs. 6 and 7). Meanwhile, the terraced slope outline, with three steps (I-II-III) in the eastern study area (Figs. 3 to 5), changes into a two-stepped morphology (I-II) in the middle (Fig. 6), and finally into an unitary steep slope (III) in the west (Fig. 7).

5. Discussion

Closure seismo-stratigraphic interpretations of 2D seismic lines enable us 1) to analyze the deep-water complex dynamics controlling the formation of the deep-water sedimentary systems described above, and 2) to investigate the spatial distribution of the deep-water sedimentary systems on the northwestern marginal slopes of the SCS Northwest Sub-Basin.

5.1. Driving forces controlling the formation of the SCS deep-water sedimentary systems

5.1.1. Bottom current activities and the SCS circulation evolution

On the gentle upper slopes in the eastern study area, where contourite channels, furrows and non-deposition features are observed, downslope *C. 1* at a water depth of ~1350 m shows an eastward migration (Fig. 8A). Similar cases of oriented migrations within downslope canyons/channels have been reported around the world (e.g., on the upper slope of the SE Brazilian margin, at the continental rise of Southeast Greenland, on the margin in the Qiongdongnan Basin and Pearl River Mouth Basin in the northern SCS), and their formations are considered due to the gravity and bottom current interacting processes (Viana et al. 1999; Rasmussen et al.

2003; Zhu et al. 2010; He et al. 2013; Li et al, 2013). The eastward oriented migration within *C. 1* is explained to be caused by the process that, the eastward flowing SIWC (roughly between 350 to 1350 m in water depths) push/force the downslope canyons migrating eastwards (Zhu et al. 2010; He et al. 2013; Li et al. 2013). Developments of the eastward canyon migrations and bottom current erosive features of contourite channels and furrows reflect relatively intense alongslope current dynamics (Hernández-Molina et al. 2008a; Stow et al. 2008). Such energetic hydrodynamics might either be caused by high velocities of the SIWC by itself, or by intensified bottom currents, constrained by an obstacle, e.g., the appearance of the SSS (Chen et al. submitted).

The development of sheeted drifts on the lower slopes below 2500 m in the eastern study area possibly indicates a wide non-focused current (Faugères and Stow 2008). Unfortunately, up till now, no detailed oceanographic information is available that may give more information on the bottom current velocities and directions in this area. Similar sheeted drifts have recently been reported in an adjacent area northeast of this study area, at water depths of ~3300 m, by Li et al. (2013). It is consider that these sheeted drifts were deposited by the westward SDWC, which is known to have the average current velocity of 0.15 m/s across the Luzon straight (Xie 2009).

The northern SCS entered deep-water settings from the early Miocene (Shao et al. 2004; Xie et al. 2011), which allows complex hydrodynamics generating various deep-water sedimentations on the marginal slopes. The seismo-stratigraphic interpretation reveals that initial contourite erosions and steady ENE migrations of *C. 1* occurred after T4 (Figs. 4 and 8A), indicating sustained bottom current activities in this area from the early Late Miocene (11.5 Ma) onwards. It is consistent with idea that the SCS thermo-haline circulation was stable from the Middle Miocene to Pliocene (Zhao 2005; Wang 2007).

Several contourite channels and the main body of sheeted drifts are recognized developing within the most recent strata (Figs. 3, 5 and 8B), where the sheeted drift deposits can be easily distinguished from underlying sediments through seismic expressions with highest amplitude and continuity, indicating widely intensified bottom current activities in the SCS during this period. Closure interpretations of 2D seismic lines help restrain these contourite deposits within the Pliocene-Quaternary strata. Within the recent 5 Ma, the SCS deep-water circulation behaviours were controlled or strongly affected by : 1) the uplifting process of Bashi Channel from ~5 Ma onwards, which blocked the SCS freely connecting to open oceans of the West Philippine Sea/the West Pacific Ocean on the eastern side (Li et al. 2007; Li et al. 2009), 2) the formation of Arctic ice caps from ~2.4 to 1.8 Ma, followed with the worldwide strengthening of deep ocean circulation and the modern phase initialization of the SCS deep water circulation (Li et al. 2009 and references therein), 3) the final formation of Bashi Channel reaching its nowadays depth of ~2400 m and the mid-Pleistocene climate transformer event at ~1 Ma, which are decisive factors for developing the final circulation pattern of the modern SCS (Li et al. 2007; Li et al. 2009; Wang and Li, 2009b; Zhao et al. 2009). Considering the highly consistent seismic reflection within the sheeted drift deposits (Figs. 3, 4, 5 and 8B), we tentatively assume that the bottom current intensifying involved might occur from the Late Pliocene onwards, in response to the start of modern phase of the SCS deep-water circulation. For further confirmations, however, more sedimentological data are required.

5.1.2. Triggering and development of slope failures

Generally, mass-transport processes of slides/slumps are prone to initiate on margins with maximum slopes (Mulder and Cochonat 1996; Lastras et al. 2006). In this study, mass-wasting deposits are distributed on slopes steeper than 2°, where is capable for causing instability and generating slope failures (Mulder 2011). The show up of reduced thickness of sediments after T4 and non-deposition features on slopes above the mass-wasting area (Figs. 3 to 6) indicates relatively low sedimentation rates. Considering the relatively low sedimentation rates, the seismic shown low seismicity and no signs for natural shallow gas or gas hydrates in this region, we suggest the steep slope be the decisive factor for triggering those mass-wasting processes (Laberg and Vorren 2000; Imbo and De Batist 2003).

The headwall scarp, which is developed in the upper part of the failure surface (where failure took place), indicates the initial vacating by displaced sediments (Hampton and Lee 1996). When 1) slides lead to instability of the upper back part of the failure surface and cause following slumps and 2) the failure surfaces of the main displaced mass is merged with that of the following slumps, successive overlapped slumps are formed (Mulder and Cochonat 1996) (Figs. 3, 4 5 and 7). Thus the headwall scarp observed on the seismic profile of Fig. 4 may indicate a latest collapse event following the lower successive overlapping slumps. Initial movement of the detached slumps could occur by back-tilting or deformation in the basal part of the slumps (Laberg and Vorren 2000). The staircase-like slumps observed in the study area are detached by a series of back-tilting failure surfaces, with small slide scars left behind (Figs. 3, 4 and 6). It hints a listric sliding of disintegrated homogeneous sediments and a retrogressive slumping pattern with the principal movement towards the SSE.

5.1.3. Factors promoting wavy sediments

Considering the developments of 1) continuous reflectors, 2) complete wave forms, 3) similar internal reflectors from one wave to the next, and 4) the upslope (NNW) migrations, we believe the wavy sediments observed in this study to be sediment waves, instead of soft sediment deformation features (e.g., creeping folds) (Wynn and Stow 2002). A sediment wave is defined as a large-scale (generally tens of metres to a few kilometres wavelength and several metres high) undulating, depositional bedforms generated beneath a current flowing at (or close to) the seafloor (Wynn et al. 2000). Commonly in deep-water environments, turbidity currents and bottom currents are referred as the main mechanisms responsible for generating sediment waves (Wynn and Stow 2002; Wynn and Masson, 2008).

In the study area, sediment waves are developed on the mid-part of the northwestern marginal slope of the Northwest Sub-Basin (~1300 to ~2000 m in water depth, ~1.3° to ~2° of slope), where submarine canyons are widely developed but bottom current depositions, e.g., sediment drifts, are missing. Specifically, sediment waves shown on seismic profiles of Fig. 8A are developed within the levee system of *C. 5*. Consulting with the summary of characteristics for different types of sediment waves by Wynn and Stow (2002), the depositional environment and medium wave dimensions (wave length < 2 km and wave height < 60 m) of the studied sediment waves, more likely, indicate a dominate wave-forming process of turbidity current. In adjacent areas, Jiang et al (2010) reported characteristics of sediment waves developed on slopes between the central canyon and the Shenhu uplift, and discussed the dominated mechanism for their origin to be overflows of turbidity currents flowing along the central canyon. Here we suppose the downslope turbidity current activities to take the main response for the generation of sediment waves reported in this paper.

5.2. Spatial distribution of deep-water sedimentary systems

Deep-water dynamic processes of downslope and alongslope current activities can shape and build continental margins, while the distribution of their sedimentary systems will in turn be influenced by various margin types (Hernández-Molina et al. 2008a, b; Stow et al. 2008; Mulder 2011 and references therein). The distribution pattern of deep-water sedimentary systems that was developed within the Pliocene-Quaternary deposits within the study area could be reconstructed (Fig. 9). This block diagram points out that, on the northwestern lower slope of the northern SCS, the composite of deep-water sedimentary systems is gradually modified from a complex of contourite erosive/depositional features, canyon and sliding deposits in the east, towards only a canyon and mass-wasting deposits in the west. This is further illustrated in Fig. 10, summarizing two deep-water sedimentary patterns based on different slope morphologies, representative for the eastern (Fig. 10 a) and western (Fig. 10b) parts of the study area.

The first pattern is based on a terraced slope in three steps (I-II-III), with the upper and lower parts of gentle slopes < 1.5° in average while the intermediate part is significantly steeper (> 2°) (Fig. 10a). Alongslope depositional processes seem to be favoured on gentle slopes where the depositional environment is stable (Hernández-Molina et al. 2008b), generating erosive features on the upper parts and sheeted drifts at lower water depths. Downslope slides/slumps and canyons are focused on the intermediate steep slope as the representative products on unstable continental slopes, whereas alongslope depositional records are commonly missing due to 1) the failure of intermediate bottom currents to erode/deposit sediments, and/or 2) the fact that alongslope depositional records are strongly affected by frequent downslope processes (Mulder et al. 2008; Stow et al. 2008). Within the second pattern (Fig. 10b), the slope outline is changed into a two-stepped terrace (I-II) outline in the east, and further into a uniform steep morphology (III) (> 2° of slope) in the west. Finally the slopes are dominated by downslope gravity flow processes of slope failures and submarine canyons, where alongslope depositional records are absent. This westward simplifying tendency of composite deep-water sedimentary systems fact is consistent with the gradually steepening slope morphology from east (< 1.5°) to west (> 2°), indicating the possible impact of slope morphology changes on deep-water depositional processes in this area. Comparable situation occurs on the Argentine Margin, where downslope depositional processes dominate the steep slopes in the north, while the Argentine Contourite System is located on the southern-most gentle sector of the Argentine continental margin (Hernández-Molina et al. 2009, 2010).

Contourite erosive features, e.g., contourite channels and furrows, indicate a bottom current with relatively high energy that enables erosions, while sheeted drifts are commonly referred to a current in lower energy that allows depositions (Hernández-Molina et al. 2008a; Faugères and Stow 2008). As discussed in 5.1.1, the contourite channels, furrows and non-deposition features appearing on the upper gentle slopes are products generated by the SIWC bottom current activities, while the sheeted drifts on the lower gentle slopes are in association with the SDWC. Thus, it hints the velocity differential between the SIWC to the SDWC, and reflects that various dynamic conditions of bottom current activities at different depths may justify specific contourite depositional products within their respective fields. Contourite depositional systems developed with multiple oceanographic conditions have been widely reported around the world, e.g., the Argentine Contourite System (circulations of the Antarctic Bottom Deep Water, North Atlantic Deep Water and Antarctic Bottom Water), the Gulf of Cadiz Contourite Depositional System (the North Atlantic Deep Water, Atlantic Inflow Water and Mediterranean Outflow Water), contourite depositional systems around the Iberian margin (the Western Mediterranean Deep Water, Levantine Intermediate Water, Mediterranean Outflow Water and Lower Deep Water in the Atlantic) (Hernández-Molina et al. 2003, 2008a, 2010, 2011b).

Moreover, it has to be noted that the apparent east-west morphological changes discussed in former texts, on the northwestern lower slopes off the Northwest Sub-Basin of the SCS, could be closely associated with the existence of the W-E oriented Xi'sha Trough on the lower part (in the south), and the appearance of the SSS on the upper part (in the east). One possibility might be that the Xi'sha Trough cuts off the lower slopes in the west and generates over steepened canyon flanks (> 4.5° in Fig. 6 and > 6.74° in Fig. 7) instead of gentle terraces (1.5° in average, Figs. 3 to 5), eliminating the required depositional environment for bottom currents. More sedimentological data are required to further address this issue, however, it is strongly hinted that the Xi'sha Trough should play a significant role in the SCS deep-water processes.

6. Conclusions

This study uses 2D multichannel reflection seismic data, combined with sedimentological data from published literatures, to investigate the depositional characteristics of a complex deep-water sedimentary system within the Pliocene and Quaternary strata on the northwestern lower slope of the Northwestern Sub-Basin, South China Sea. The main conclusions of this study are:

1. During the Pliocene-Quaternary, a complex and composite deep-water sedimentary system has been developed on the northwestern middle-lower slope (~1000 to ~3500 m in water depth) of the Northwestern

Sub-Basin of the SCS.

2. Alongslope depositional systems developed on gentle slopes (< 1.5° in average) in the eastern part, with alongslope aligned erosive features (contourite channels, furrows and non-deposition features) at water depth < 1500 m possibly generated by the eastwards SIWC, and sheeted drifts at water depth > 2500 m possibly generated by the westwards SIWC.
3. Downslope gravity flow activities dominate the depositional processes on steep slopes (> 2°), generating submarine canyons and mass-wasting deposits of headwall scarp, successive overlapped slumps and failure surfaces, slide scars and detached slumps, at water depths ranging from ~1500 to ~2000 m in the east and ~1250 to ~2250 m in the west. Turbidity current activities are suggested to take the main response for the generation of sediment waves (wave lengths < 2 km and wave heights < 60 m), which are developed on slopes (1.3° to 2°) ranging from ~1800 to ~2000 m in water depths and show continuous reflectors, complete wave forms and upslope (NNW) migrations.
4. The composite of deep-water system is modified from east to west, from a complex of contourite erosive/depositional features, slope failures and canyons in the east, towards only mass-wasting and canyon depositions in the west, which is in close association with the steepening of slope morphologies from east to west in the study area.

Acknowledgements The study was supported by the National Natural Science Foundation of China (No. 91028009), the Key project of Hubei Natural Science Foundation (No.2008CDA095), the Ph.D. Program Foundation of Ministry of Education (No. 20100145110002) and the National Key Projects of Oil and Gas (No.2011ZX05025-002-02). This article is also a contribution to IGCP project 619 and INQUA project 1204. We would like to acknowledge the Institute of Petroleum Exploration and Development, Nanhai West Oil Corporation for providing geophysical data. The exchange-student programme for H. Chen was framed under the Cooperation Agreement between the China University of Geosciences (P.R. China) and Ghent University (Belgium). We appreciate Mr. Jing-Liang Guo's help for English improvement. We thank the reviewers for their comments that significantly improved the manuscript.

References

Bouma AH (1964) Turbidites. In: Bouma AH, Brouwer A (eds) Turbidites. Developments in Sedimentology, vol 3. Elsevier, Amsterdam, pp 247-256. doi:10.1016/S0070-4571(08)70967-1

Chen C-TA (2005) Tracing tropical and intermediate waters from the South China Sea to the Okinawa Trough and beyond. J Geophys Res-Oceans 110 (C5):C05012. doi:10.1029/2004JC002494

Chen C-TA, Wang S-L (1998) Influence of intermediate water in the western Okinawa Trough by the outflow from the South China Sea. J Geophys Res-Oceans 103 (C6):12683-12688. doi:10.1029/98JC00366

Chen H, Xie X, Van Rooij D, Vandorpe T, Su M. Depositional characteristics and processes of alongslope currents related to a seamount on the northwestern margin of the Northwest Sub-Basin, South China Sea. Submitted to Mar Geol.

Chen PPH, Chen ZY, Zhang QM (1993) Sequence stratigraphy and continental-margin development of the northwestern shelf of the South China Sea. AAPG bulletin 77 (5):842-862.

Fang G, Fang W, Fang Y, Wang K (1998) A survey of studies on the South China Sea upper ocean circulation. Acta Oceanogr Taiwan 37 (1):1-16.

Faugères J-C, Mulder T (2011) Chapter 3 - Contour Currents and Contourite Drifts. In: Hüneke H, Mulder T (eds) Deep-Sea Sediments. Developments in Sedimentology, vol 63. Elsevier, Amsterdam, pp 149-214. doi:10.1016/B978-0-444-53000-4.00003-2

Faugères J-C, Stow DAV (2008) Chapter 14 - Contourite Drifts: Nature, Evolution and Controls. In: Rebesco M, Camerlenghi A (eds) Contourites. Developments in Sedimentology, vol 60. Elsevier, Amsterdam, pp

257-288. doi:10.1016/S0070-4571(08)10014-0

Faugères J-C, Stow DAV, Imbert P, Vianna A (1999) Seismic features diagnostic of contourite drifts. Marine Geology 162 (1):1-38. doi:10.1016/S0025-3227(99)00068-7

Frigola J, Moreno A, Cacho I, Canals M, Sierro FJ, Flores JA, Grimalt JO (2008) Evidence of abrupt changes in Western Mediterranean Deep Water circulation during the last 50 kyr: A high-resolution marine record from the Balearic Sea. Quatern Int 181 (1):88-104. doi:10.1016/j.quaint.2007.06.016

Gong C, Wang Y, Peng X, Li W, Qiu Y, Xu S (2012) Sediment waves on the South China Sea Slope off southwestern Taiwan: Implications for the intrusion of the Northern Pacific Deep Water into the South China Sea. Mar Petrol Geol 32 (1):95-109. doi:10.1016/j.marpetgeo.2011.12.005

Hampton MA, Lee HJ, Jacques L (1996) Submarine landslides. Reviews of Geophysics 34 (1):33-59. doi:10.1029/95RG03287

He Y, Xie X, Kneller BC, Wang Z, Li X (2013) Architecture and controlling factors of canyon fills on the shelf margin in the Qiongdongnan Basin, northern South China Sea. Mar Petrol Geol 41:264-276. doi:10.1016/j.marpetgeo.2012.03.002

Hernández-Molina FJ, Llave E, Somoza L, Fernandez-Puga MC, Maestro A, Leon R, Medialdea T, Barnolas A, Garcia M, del Rio VD, Fernandez-Salas LM, Vazquez JT, Lobo F, Dias JMA, Rodero J, Gardner J (2003) Looking for clues to paleoceanographic imprints: A diagnosis of the Gulf of Cadiz contourite depositional systems. Geology 31 (1):19-22. doi:10.1130/0091-7613(2003)031<0019:LFCTPI>2.0.CO;2

Hernández-Molina FJ, Llave E, Stow DAV (2008a) Chapter 19 Continental Slope Contourites. In: Rebesco M, Camerlenghi A (eds) Contourites. Developments in Sedimentology, vol 60. Elsevier, Amsterdam, pp 379-408. doi:10.1016/S0070-4571(08)10019-X

Hernández-Molina FJ, Llave E, Stow DAV, García M, Somoza L, Vázquez JT, Lobo FJ, Maestro A, Díaz del Río V, León R, Medialdea T, Gardner J (2006) The contourite depositional system of the Gulf of Cádiz: A sedimentary model related to the bottom current activity of the Mediterranean outflow water and its interaction with the continental margin. Deep Sea Res Part II 53 (11–13):1420-1463. doi:10.1016/j.dsr2.2006.04.016

Hernández-Molina FJ, Maldonado A, Stow DAV (2008b) Chapter 18 Abyssal Plain Contourites. In: Rebesco M, Camerlenghi A (eds) Contourites. Developments in Sedimentology, vol 60. Elsevier, Amsterdam, pp 345-378. doi:10.1016/S0070-4571(08)10018-8

Hernández-Molina FJ, Paterlini M, Somoza L, Violante R, Arecco MA, de Isasi M, Rebesco M, Uenzelmann-Neben G, Neben S, Marshall P (2010) Giant mounded drifts in the Argentine Continental Margin: Origins, and global implications for the history of thermohaline circulation. Mar Petrol Geol 27 (7):1508-1530. doi:10.1016/j.marpetgeo.2010.04.003

Hernández-Molina FJ, Paterlini M, Violante R, Marshall P, de Isasi M, Somoza L, Rebesco M (2009) Contourite depositional system on the Argentine Slope: An exceptional record of the influence of Antarctic water masses. Geology 37 (6):507-510. doi:10.1130/G25578a.1

Hernández-Molina FJ, Serra N, Stow D, Llave E, Ercilla G, Van Rooij D (2011) Along-slope oceanographic processes and sedimentary products around the Iberian margin. Geo-Marine Letters 31 (5-6):315-341. doi:10.1007/s00367-011-0242-2

Hernández-Molina FJ, Stow DAV, Llave E, Rebesco M, Ercilla G, Rooij D, Mena A, Vázquez J-T, Voelker AL (2011a) Deep-water Circulation: Processes & Products (16–18 June 2010, Baiona): introduction and future challenges. Geo-Mar Lett 31 (5-6):285-300. doi:10.1007/s00367-011-0261-z

Imbo Y, De Batist M, Canals M, Prieto MJ, Baraza J (2003) The Gebra Slide: a submarine slide on the Trinity Peninsula Margin, Antarctica. Marine Geology 193 (3-4):235-252. doi:10.1016/S0025-3227(02)00664-3

Jiang T, Zhang Y, Xie X, Ren J, Zhang C (2010) Characteristics and origin of sediment waves in the Qiongdongnan Basin, northern South China Sea. Geo-Temas 11:193-194.

Laberg JS, Vorren TO (2000) The Trænadjupet Slide, offshore Norway-morphology, evacuation and triggering mechanisms. Marine Geology 171 (1-4):95-114. doi:10.1016/S0025-3227(00)00112-2

Lastras G, Canals M, Amblas D, Ivanov M, Dennielou B, Droz L, Akhmetzhanov A (2006) Eivissa slides, western Mediterranean Sea: morphology and processes. Geo-Marine Letters 26 (4):225-233. doi: 10.1007/s00367-006-0032-4

Li H, Wang Y, Zhu W, Xu Q, He Y, Tang W, Zhuo H, Wang D, Wu J, Li D (2013) Seismic characteristics and processes of the Plio-Quaternary unidirectionally migrating channels and contourites in the northern slope of the South China Sea. Mar Petrol Geol. doi:10.1016/j.marpetgeo.2012.12.010

Li Q, Zhao Q, Zhong G, Jian Z, Tian J, Cheng X, Chen M (2007) Deep water ventilation and stratification in the Neogene South China Sea. Earth Science 18 (2):95-108.

Li Q, Zhong G, Tian J (2009) Stratigraphy and Sea Level Changes. In: Wang P, Li Q (eds) The South China Sea. Developments in Paleoenvironmental Research, vol 13. Springer, Netherlands, pp 75-170. doi:10.1007/978-1-4020-9745-4_3

Liu Z, Huang W, Li J, Wang P, Wang R, Yu K, Zhao J (2009) Sedimentology. In: Wang P, Li Q (eds) The South China Sea. Developments in Paleoenvironmental Research, vol 13. Springer, Netherlands, pp 171-295. doi:10.1007/978-1-4020-9745-4_4

Lüdmann T, Kin Wong H, Wang P (2001) Plio-Quaternary sedimentation processes and neotectonics of the northern continental margin of the South China Sea. Mar Geol 172 (3–4):331-358. doi:10.1016/S0025-3227(00)00129-8

Lüdmann T, Wong HK, Berglar K (2005) Upward flow of North Pacific Deep Water in the northern South China Sea as deduced from the occurrence of drift sediments. Geophys Res Lett 32 (5):L05614. doi:10.1029/2004GL021967

Mulder T (2011) Chapter 2 - Gravity Processes and Deposits on Continental Slope, Rise and Abyssal Plains. In:

Hüneke H, Mulder T (eds) Deep-Sea Sediments. Developments in Sedimentology, vol 63. Elsevier, Amsterdam, pp 25-148. doi:10.1016/B978-0-444-53000-4.00002-0

Mulder T, Cochonat P (1996) Classification of offshore mass movements. Journal of Sedimentary Research 66 (1):43-57. doi: 10.1306/D42682AC-2B26-11D7-8648000102C1865D

Mulder T, Faugères JC, Gonthier E (2008) Chapter 21 Mixed Turbidite-Contourite Systems. In: Rebesco M, Camerlenghi A (eds) Contourites. Developments in Sedimentology, vol 60. Elsevier, Amsterdam, pp 435-456. doi:10.1016/S0070-4571(08)10021-8

Mulder T, Hüneke H, Van Loon AJ (2011) Chapter 1-Progress in Deep-Sea Sedimentology. In: Hüneke H, Mulder T (eds) Deep-Sea Sediments. Developments in Sedimentology, vol 63. Elsevier, Amsterdam, pp 1-24. doi:10.1016/B978-0-444-53000-4.00001-9

Qu T, Girton JB, Whitehead JA (2006) Deepwater overflow through Luzon Strait. J Geophys Res-Oceans 111 (C1):C01002. doi:10.1029/2005JC003139

Qu T, Lindstrom EJ (2004) Northward Intrusion of Antarctic Intermediate Water in the Western Pacific. J Phys Oceanogr 34 (9):2104-2118. doi:10.1175/1520-0485(2004)034<2104:NIOAIW>2.0.CO;2

Rasmussen S, Lykke-Andersen H, Kuijpers A, Troelstra SR (2003) Post-Miocene sedimentation at the continental rise of Southeast Greenland: the interplay between turbidity and contour currents. Marine Geology 196 (1-2):1-16. doi:10.1016/S0025-3227(03)00043-4

Shao L, Li X, Geng J, Pang X, Lei Y, Qiao P, Wang L, Wang H (2007) Deep water bottom current deposition in the northern South China Sea. Sci China Ser D 50 (7):1060-1066. doi:10.1007/s11430-007-0015-y

Shao L, Li X, Wang P, Jian Z, Wei G, Pang X, Liu Y (2004) Sedimentary record of the tectonic evolution of the South China Sea since the Oligocene-Evidence from deep sea sediments of ODP Site 1148. Adv Earth Sci 19 (4):539-544

Stow DAV, Hunter S, Wilkinson D, Hernández-Molina FJ (2008) Chapter 9 The Nature of Contourite

Deposition. In: Rebesco M, Camerlenghi A (eds) Contourites. Developments in Sedimentology, vol 60. Elsevier, Amsterdam, pp 143-156. doi:10.1016/S0070-4571(08)10009-7

Sun Z, Zhong Z, Keep M, Zhou D, Cai D, Li X, Wu S, Jiang J (2009) 3D analogue modeling of the South China Sea: A discussion on breakup pattern. J Asian Earth Sci 34 (4):544-556. doi:10.1016/j.jseaes.2008.09.002

Sun Z, Zhou D, Zhong Z, Xia B, Qiu X, Zeng Z, Jiang J (2006) Research on the dynamics of the South China Sea opening: Evidence from analogue modeling. Sci China Ser D 49 (10):1053-1069. doi:10.1007/s11430-006-1053-6

Tian J, Qu T (2012) Advances in research on the deep South China Sea circulation. Chin Sci Bull 57 (24):3115-3120. doi:10.1007/s11434-012-5269-x

Varnes DJ (1978) Slope movement types and processes. In: Schuster RL, Krizek RJ (eds) Landslides-Analysis and Control. Transp Res Board, Spec Rep 176, Natl Res Counc, Washington, D.C., pp 12-33.

Viana AR, Almeida JW, Machado LC (1999) Different styles of canyon infill related to gravity and bottom current processes: Example from the upper slope of the SE Brazilian Margin. In: 6th Int Cong of the Brazil. Geophys. Soc, Rio De Janeiro, p. SBGF0199.

Wang D, Wang Q, Zhou W, Cai S, Li L, Hong B (2013) An analysis of the current deflection around Dongsha Islands in the northern South China Sea. Journal of Geophysical Research: Oceans 118 (1):490-501. doi:10.1029/2012JC008429

Wang H (2007) Sedimentation processes and its response in deep-water environment of the northern continental margin, the South China Sea. Ph.D. thesis, China University of Petroleum, Beijing

Wang H, Yuan S, Gao H (2010) The contourite system and the framework of contour current circulation in the South China Sea. Geo-Temas 11:179-180

Wang P, Li Q (2009a) Introduction. In: Wang P, Li Q (eds) The South China Sea. Developments in Paleoenvironmental Research, vol 13. Springer, Netherlands, pp 1-23. doi:10.1007/978-1-4020-9745-4_1

Wang P, Li Q (2009b) Oceanographical and Geological Background. In: Wang P, Li Q (eds) The South China Sea. Developments in Paleoenvironmental Research, vol 13. Springer, Netherlands, pp 25-73. doi:10.1007/978-1-4020-9745-4_2

Wang P, Prell W, Blum P, al e (2000) Proc. ODP, Init. Repts., 184: College Station, TX (Ocean Drilling Program). doi:10.2973/odp.proc.ir.184.2000

Wynn RB, Masson DG (2008) Chapter 15-Sediment Waves and Bedforms. In: Rebesco M, Camerlenghi A, (eds) Developments in Sedimentology, vol 60. Elsevier, pp 289-300. doi:10.1016/S0070-4571(08)10015-2

Wynn RB, Stow DAV (2002) Classification and characterisation of deep-water sediment waves. Marine Geology 192 (1-3):7-22. doi: 10.1016/S0025-3227(02)00547-9

Wynn RB, Weaver PPE, Ercilla G, Stow DAV, Masson DG (2000) Sedimentary processes in the Selvage sediment-wave field, NE Atlantic: new insights into the formation of sediment waves by turbidity currents. Sedimentology 47 (6):1181-1197. doi:10.1046/j.1365-3091.2000.00348.x

Xie L (2009) Study on the circulation in Western North Pacific and the water exchange between the Pacific and the South China Sea. Ph.D thesis, Ocean University of China, Qingdao.

Xie Q, Xiao JG, Wang DX, Yu YQ (2013) Analysis of deep-layer and bottom circulations in the South China Sea based on eight quasi-global ocean model outputs. Chin Sci Bull 58 (1):1-7. doi:10.1007/s11434-013-5791-5

Xie X, Zhang C, Ren J, Yao B, Wan L, Chen H, Kang B (2011) Effects of distinct tectonic evolutions on hydrocarbon accumulation in northern and southern continental marginal basins of South China Sea. Chin J Geophys-Ch 54 (12):3280-3291. doi:10.3969/j.issn.0001-5733.2011.12.026

Xue H, Chai F, Pettigrew N, Xu D, Shi M, Xu J (2004) Kuroshio intrusion and the circulation in the South China Sea. J Geophys Res-Oceans 109 (C2):C02017. doi:10.1029/2002JC001724

Yuan D (2002) A numerical study of the South China Sea deep circulation and its relation to the Luzon Strait transport. Acta Oceanol Sin 21 (2):187-202.

Yuan S (2009) Sedimentary system of deepwater channel, the slope area of northern South China Sea. Ph.D thesis, Insititue of Oceanology, Chinese Academy of Sciences, Qingdao

Zhao Q (2005) Late Cainozoic ostracod faunas and paleoenvironmental changes at ODP Site 1148, South China Sea. Marine Micropaleontology 54 (1-2):27-47. doi: 10.1016/j.marmicro.2004.09.002

Zhao Q, Li Q, Jian Z (2009) Deep waters and oceanic connection. In: Wang P, Li Q (eds) The South China Sea. Springer, Netherlands, pp 395-437. doi: 10.1007/978-1-4020-9745-4_6

Zheng H-B, Yan P (2012) Deep-Water Bottom Current Research in the Northern South China Sea. Mar Georesour Geotec 30 (2):122-129. doi:10.1080/1064119X.2011.586015

Zhu M, Graham S, Pang X, McHargue T (2010) Characteristics of migrating submarine canyons from the middle Miocene to present: Implications for paleoceanographic circulation, northern South China Sea. Mar Petrol Geol 27 (1):307-319. doi:10.1016/j.marpetgeo.2009.05.005

Figure captions

Fig. 1 (**A)** Overview map of the mid-northern part of the South China Sea (SCS), with the locations of the sedimentary basins, as well as the main local structures (Sun et al. 2009; Yuan 2009; Zhu et al. 2010; Wang 2007). The four dots in yellow represent the drilling locations of 1) ODP sites 1144, 1146 and 1148 (Lüdmann et al. 2001; Wang et al. 2000) and 2) an industrial well W1. The two dotted lines in yellow represent the locations of through-well seismic lines: 1) the eastern seismic line connects ODP sites 1146 and 1146, and it is illustrated in Fig. 1B; 2) the western seismic line ties the industrial well W1 to the study area (red square), which contains the seismic profile of Fig. 3 as its southeastern section. The study area (red square) is located on the northwestern margin of the Northwest Sub-Basin (Fig2). The red arrows are the pathways for the intrusion of the Northern Pacific Deep Water into SCS via the Bashi Channel and the Luzon Strait (modified from Gong et al. 2012; Lüdmann et al. 2005); The pink arrows are possible deep current circulation pathways in the mid-northern SCS (Shao et al. 2007; Wang et al. 2010; Zheng and Yan 2012). The yellow star on the submarine canyon that connects with the Xi'sha Trough indicates the location of the Central Canyon in the Qiongdongnan Basin. The inset (middle left) is the regional setting of the SCS (modified from Sun et al. 2009). (**B)** Interpretation of the seismic profile connecting ODP sites 1146 and 1148 (modified from Lüdmann et al. 2001; Wang et al. 2000; Li et al. 2013); Q = Quaternary; P = Pliocene; M = Miocene; O = Oligocene

Fig. 2 Bathymetry of the study area showing the locations of the 2D seismic profiles covered in the study area; the thick solid lines in white show the locations of profiles in **Figs. 3 to 8**; the dashed lines in yellow show the locations of submarine canyons (*C. 1* to *C. 6*) covering in this paper; SSS = the South Shenhu Seamount

Fig. 3 NNW-SSE oriented profile showing contourite channels and non-deposition features, sheeted drift, mass-wasting deposits (successive overlapped slumps, failure surfaces, slide scar and detached slumps), and submarine canyon *C. 1*, on the terraced slopes with three steps of I (slope < 1.13°), II (slope > 3.3°) and III (slope of ~0.61° to ~2.45°) in the eastern study area

Fig. 4 NNW-SSE oriented profile showing contourite channels and non-deposition features, sheeted drift, mass-wasting deposits (headwall scarp, successive overlapped slumps, failure surfaces, slide scar and detached slumps), and submarine canyon *C. 1*, on the terraced slopes with three steps of I (slope < 1.14°), II (slope of ~2.35° to ~3.94°) and III (slope < 1.54°) in the eastern study area

Fig. 5 NNW-SSE oriented profile showing contourite channels and non-deposition features, mass-wasting deposits (successive overlapped slumps and failure surfaces), wavy sediments, contourite sheeted drifts, and submarine canyon *C. 2*, *C. 3* and *C. 4*, on the terraced slopes with three steps of I (slope < 0.875°), II (slope of ~1.32° to ~2.84°) and III (slope < 1°) in the eastern study area

Fig. 6 NNW-SSE oriented profile showing contourite furrow and non-deposition features, mass-wasting deposits (successive overlapped slumps, failure surfaces, slide scar and detached slumps), on the terraced slopes with two steps of I (slope < 1.05°), II (slope of ~1.1° to ~2.57°) in the western study area; the submarine canyon *C. 2* is shown on the over steepened slopes (slope > 4.5°), where is a slide scar on the upper flank of the Xi'sha Trough

Fig. 7 NNW-SSE oriented profile showing mass-wasting deposits (successive overlapped slumps and failure surfaces), wavy sediments, and submarine canyons *C'*, *C"* and *C. 5* on the slopes with a uniform steep morphology II (slope > 2.07°) in the western study area; the over steepened slopes (slope > 6.74°) belong to the upper flank of the Xi'sha Trough

Fig. 8 **A** WSW-ENE oriented profile showing the downslope submarine canyon *C. 1* on the eastern upper slopes of the study area, with a water depth of ~1350 m and slope < 1.14°; the solid arrow in black represents an obvious ENE migration of *C. 1*. **B** WSW-ENE oriented profile showing sheeted drift and submarine canyons of *C. 4* and *C. 6* in the eastern lower slopes, with water depths of ~2600 to ~3000 m and slopes of < 1 ° for sheeted drift and > 5.0° for canyons. **C** WSW-ENE oriented profile showing wavy sediments, and the downslope submarine canyon of *C. 5* with its levee system, on the western intermediate slopes with a water depth of ~1800 m and slope ~2.07°

Fig. 9 Block diagram showing the distribution pattern of deep-water sedimentary systems that was developed over the Pliocene Quaternary in the study area; *C. 1* to *C. 6* = Canyon 1 to Canyon 6; SSS = the South Shenhu Seamount; the solid arrow in green represents the possible eastwards South China Sea (SCS) Intermediate Water Circulation (SIWC); the solid arrows in blue represent the possible westwards SCS Deep Water Circulation (SDWC); the dashed line in black represent the marginal fault

Fig. 10 Deep-water sedimentary patterns based on the two slope morphologies representative for the eastern (**A**) and western (**B**) parts of the study area

FIG. 1

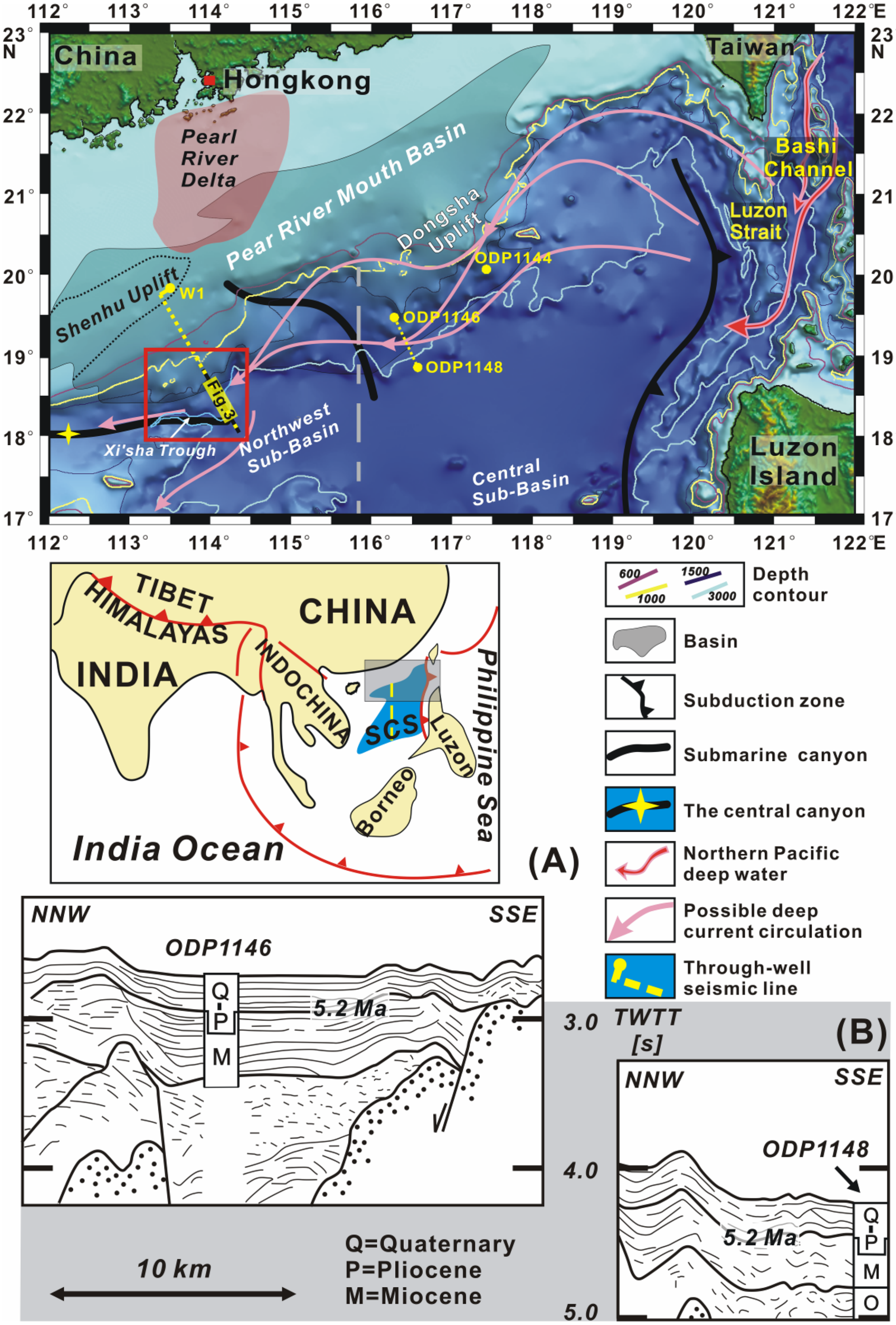

China
Hongkong
Taiwan
Pearl River Delta
Pear River Mouth Basin
Dongsha Uplift
Bashi Channel
Luzon Strait
ODP1144
Shenhu Uplift
W1
ODP1146
ODP1148
Fig.3
Xi'sha Trough
Northwest Sub-Basin
Central Sub-Basin
Luzon Island
TIBET
HIMALAYAS
CHINA
INDIA
INDOCHINA
SCS
Luzon
Philippine Sea
Borneo
India Ocean
(A)
Depth contour
600
1000
1500
3000
Basin
Subduction zone
Submarine canyon
The central canyon
Northern Pacific deep water
Possible deep current circulation
Through-well seismic line
NNW
SSE
Q
P
M
O
5.2 Ma
3.0
4.0
5.0
TWTT [s]
(B)
10 km
Q=Quaternary
P=Pliocene
M=Miocene

FIG. 2

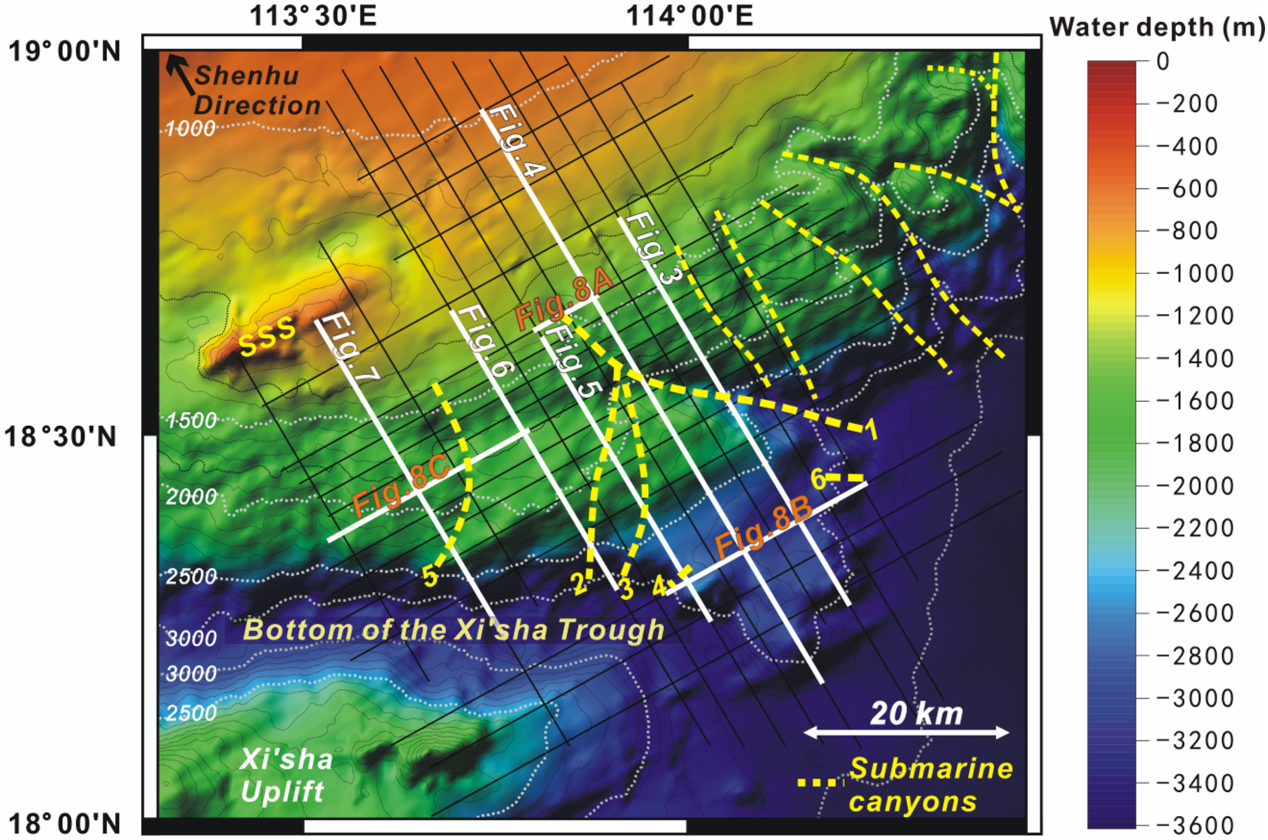

113° 30'E
114° 00'E
Water depth (m)
19° 00'N
18°30'N
18° 00'N
Shenhu Direction
1000
1500
2000
2500
3000
3000
2500
SSS
Fig.4
Fig.3
Fig.7
Fig.6
Fig.5
Fig.8A
Fig.8B
Fig.8C
1
2
3
4
5
6
Bottom of the Xi'sha Trough
Xi'sha Uplift
20 km
Submarine canyons
0
-200
-400
-600
-800
-1000
-1200
-1400
-1600
-1800
-2000
-2200
-2400
-2600
-2800
-3000
-3200
-3400
-3600

FIG. 3

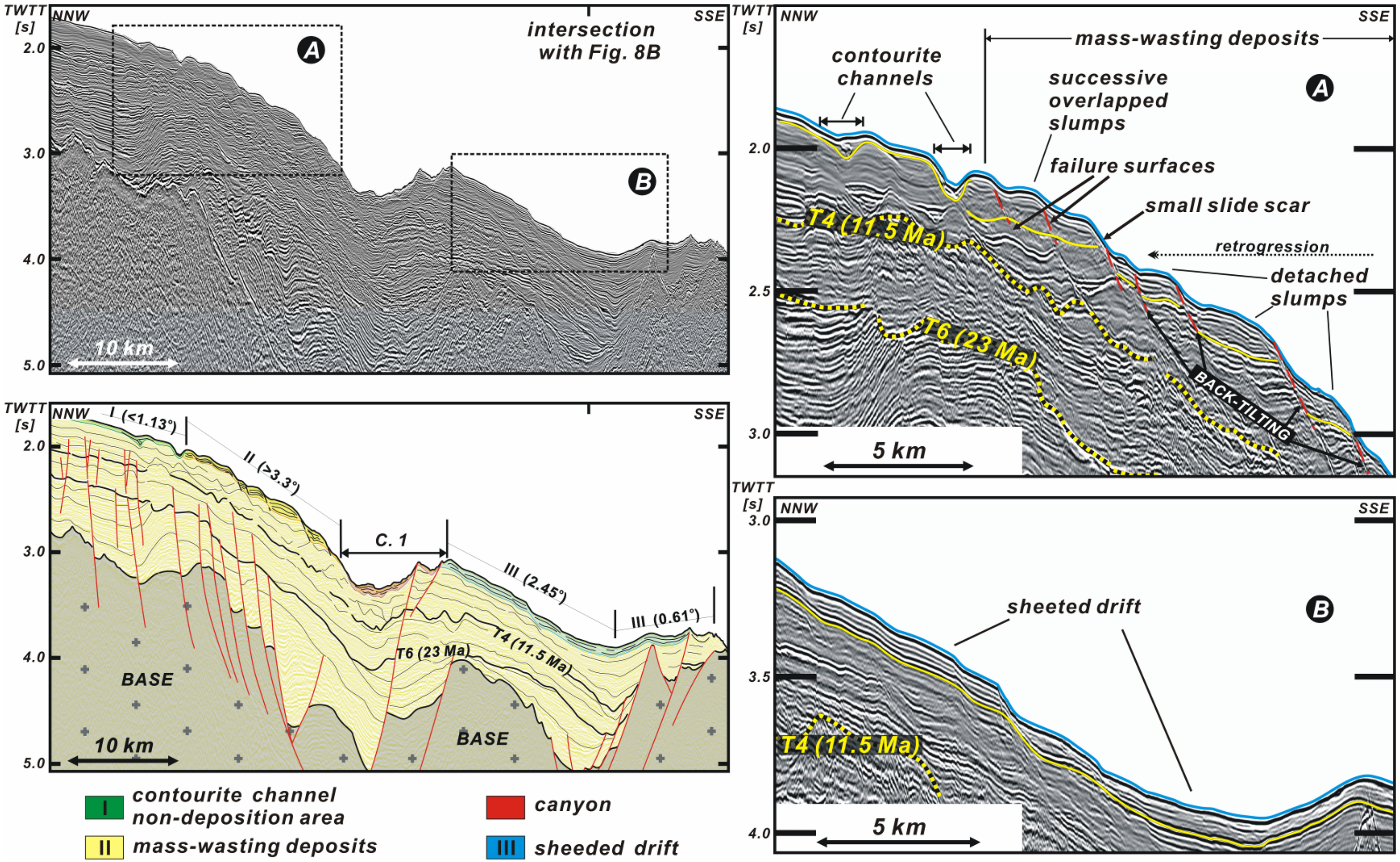

TWTT [s]
NNW
SSE
intersection with Fig. 8B
A
B
10 km
2.0
3.0
4.0
5.0
I (<1.13°)
II (>3.3°)
C. 1
III (2.45°)
III (0.61°)
T6 (23 Ma)
T4 (11.5 Ma)
BASE
BASE
10 km
contourite channel non-deposition area
mass-wasting deposits
canyon
sheeded drift
contourite channels
mass-wasting deposits
successive overlapped slumps
failure surfaces
small slide scar
retrogression
detached slumps
T4 (11.5 Ma)
T6 (23 Ma)
BACK-TILTING
5 km
2.5
sheeted drift
T4 (11.5 Ma)
3.5
5 km

FIG. 4

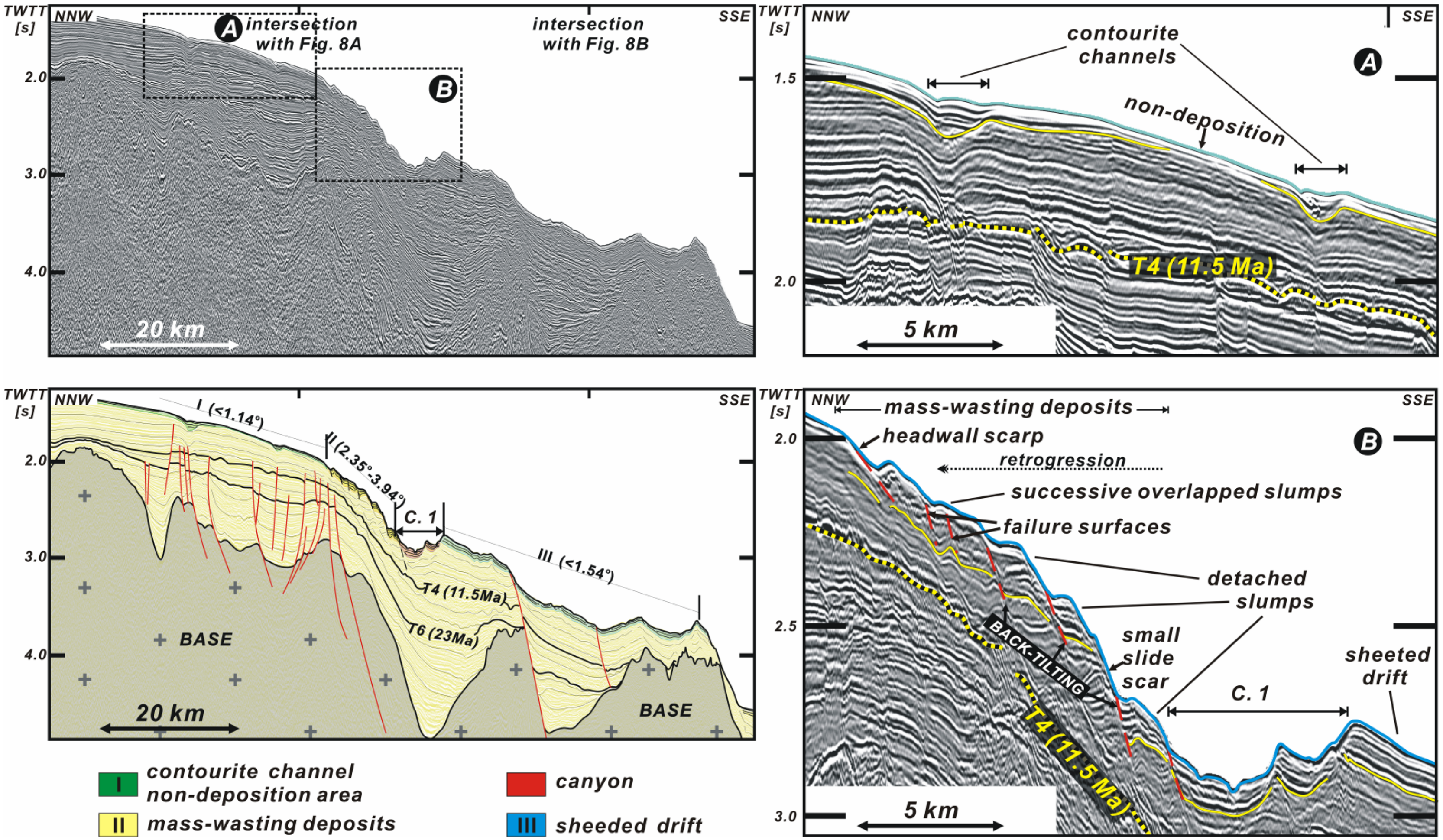
TWTT [s]
NNW
SSE
intersection with Fig. 8A
intersection with Fig. 8B
A
B
2.0
3.0
4.0
20 km
1.5
contourite channels
non-deposition
T4 (11.5 Ma)
5 km
I (<1.14°)
II (2.35°-3.94°)
C. 1
III (<1.54°)
T4 (11.5Ma)
T6 (23Ma)
BASE
mass-wasting deposits
headwall scarp
retrogression
successive overlapped slumps
failure surfaces
detached slumps
small slide scar
BACK-TILTING
sheeted drift
2.5
I contourite channel non-deposition area
II mass-wasting deposits
canyon
III sheeded drift

FIG. 5

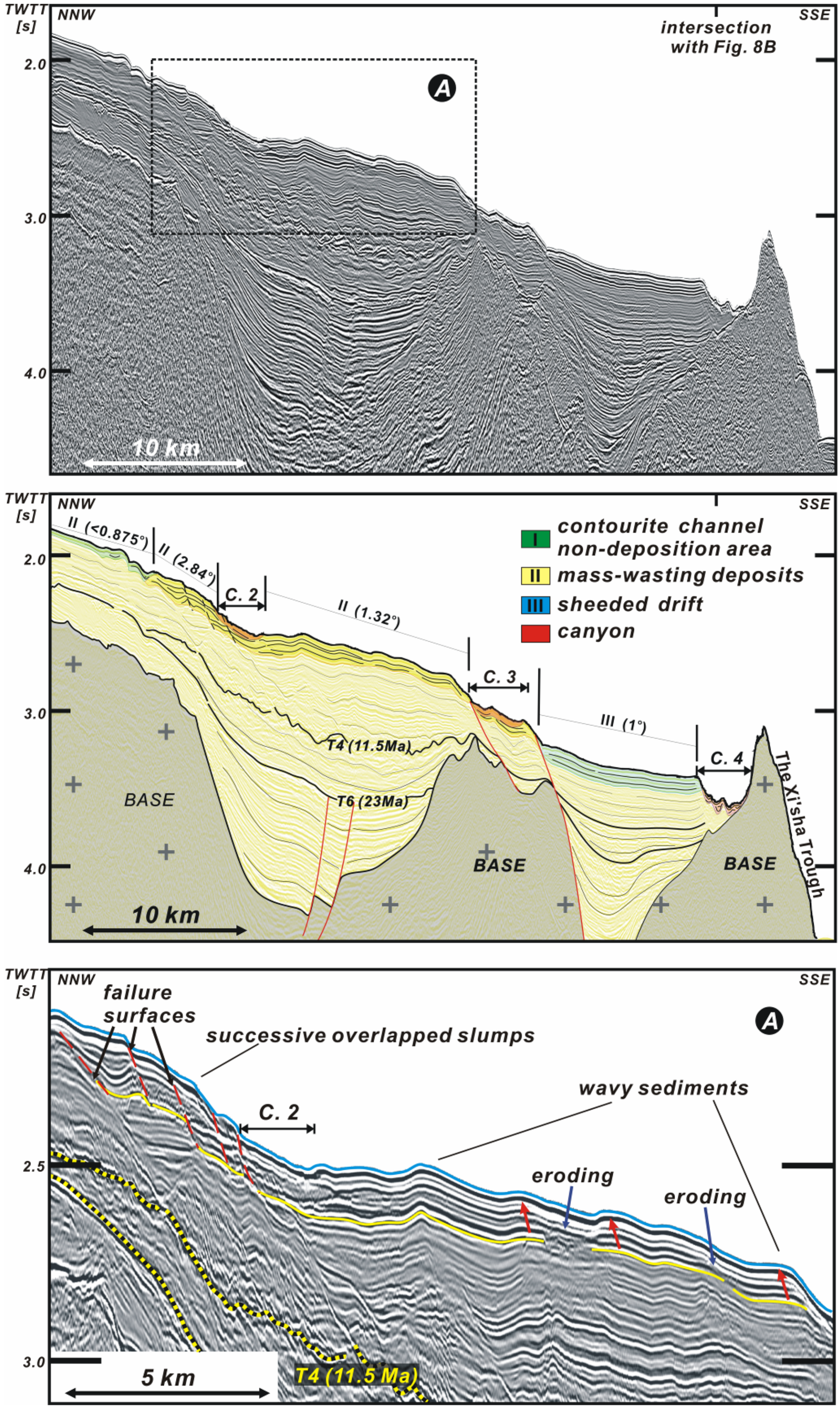
TWTT [s]
NNW
SSE
intersection with Fig. 8B
A
2.0
3.0
4.0
10 km
II (<0.875°)
II (2.84°)
C. 2
II (1.32°)
C. 3
III (1°)
C. 4
I contourite channel non-deposition area
II mass-wasting deposits
III sheeded drift
canyon
T4 (11.5Ma)
T6 (23Ma)
BASE
The Xi'sha Trough
failure surfaces
successive overlapped slumps
wavy sediments
eroding
2.5
5 km
T4 (11.5 Ma)

FIG. 6

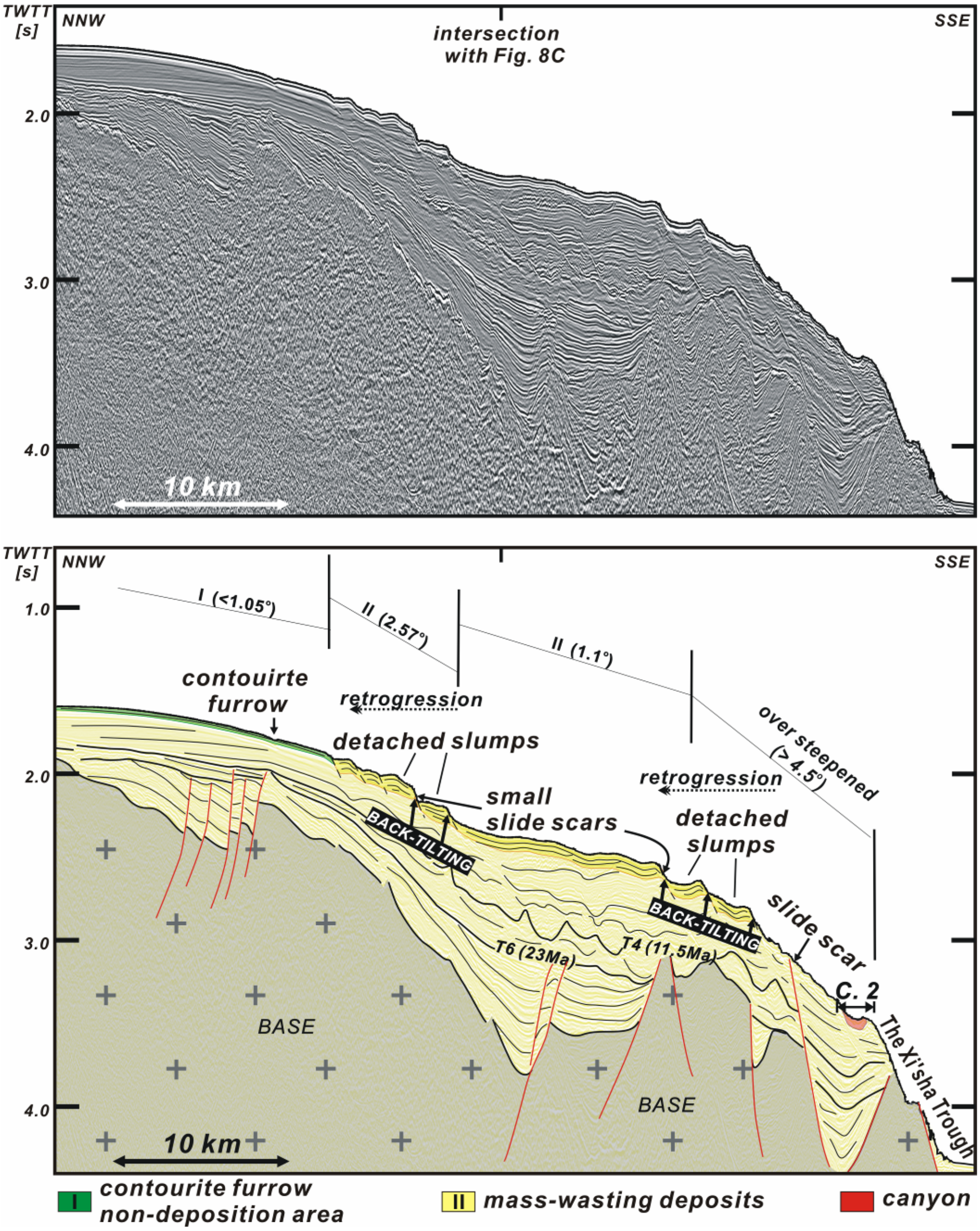
TWTT [s]
NNW
SSE
intersection with Fig. 8C
2.0
3.0
4.0
10 km
TWTT [s]
NNW
SSE
1.0
I (<1.05°)
II (2.57°)
II (1.1°)
over steepened (> 4.5°)
contouirte furrow
retrogression
detached slumps
small slide scars
BACK-TILTING
retrogression
detached slumps
BACK-TILTING
slide scar
C. 2
The Xi'sha Trough
T6 (23Ma)
T4 (11.5Ma)
BASE
BASE
2.0
3.0
4.0
10 km
I contourite furrow non-deposition area
II mass-wasting deposits
canyon

FIG. 7

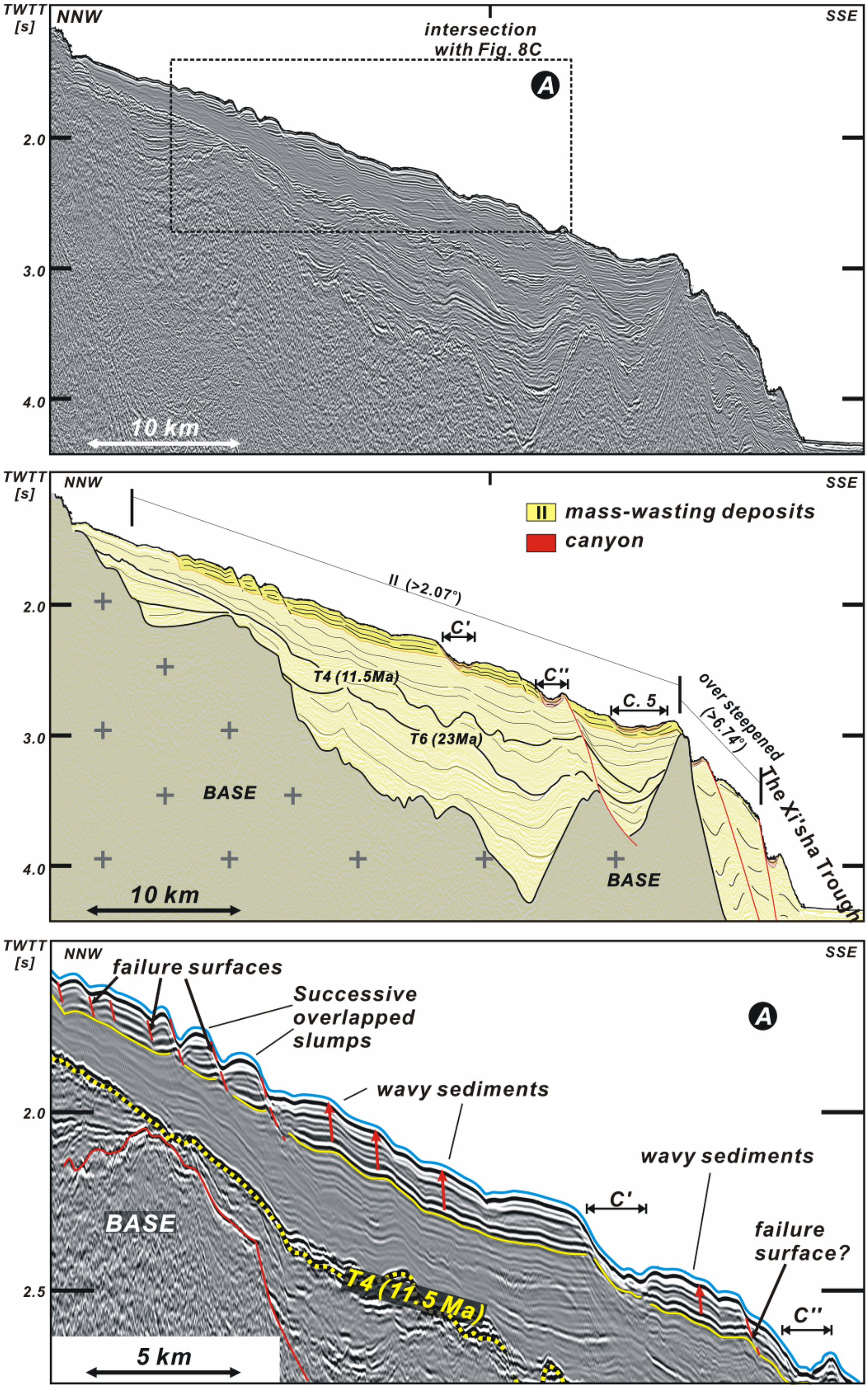

TWTT [s]
NNW
SSE
intersection with Fig. 8C
A
2.0
3.0
4.0
10 km
TWTT [s]
NNW
SSE
mass-wasting deposits
canyon
II (>2.07°)
C'
C''
C. 5
T4 (11.5Ma)
T6 (23Ma)
over steepened (>6.74°)
The Xi'sha Trough
BASE
BASE
2.0
3.0
4.0
10 km
TWTT [s]
NNW
SSE
failure surfaces
Successive overlapped slumps
A
wavy sediments
wavy sediments
C'
failure surface?
C''
BASE
T4 (11.5 Ma)
2.0
2.5
5 km

FIG. 8

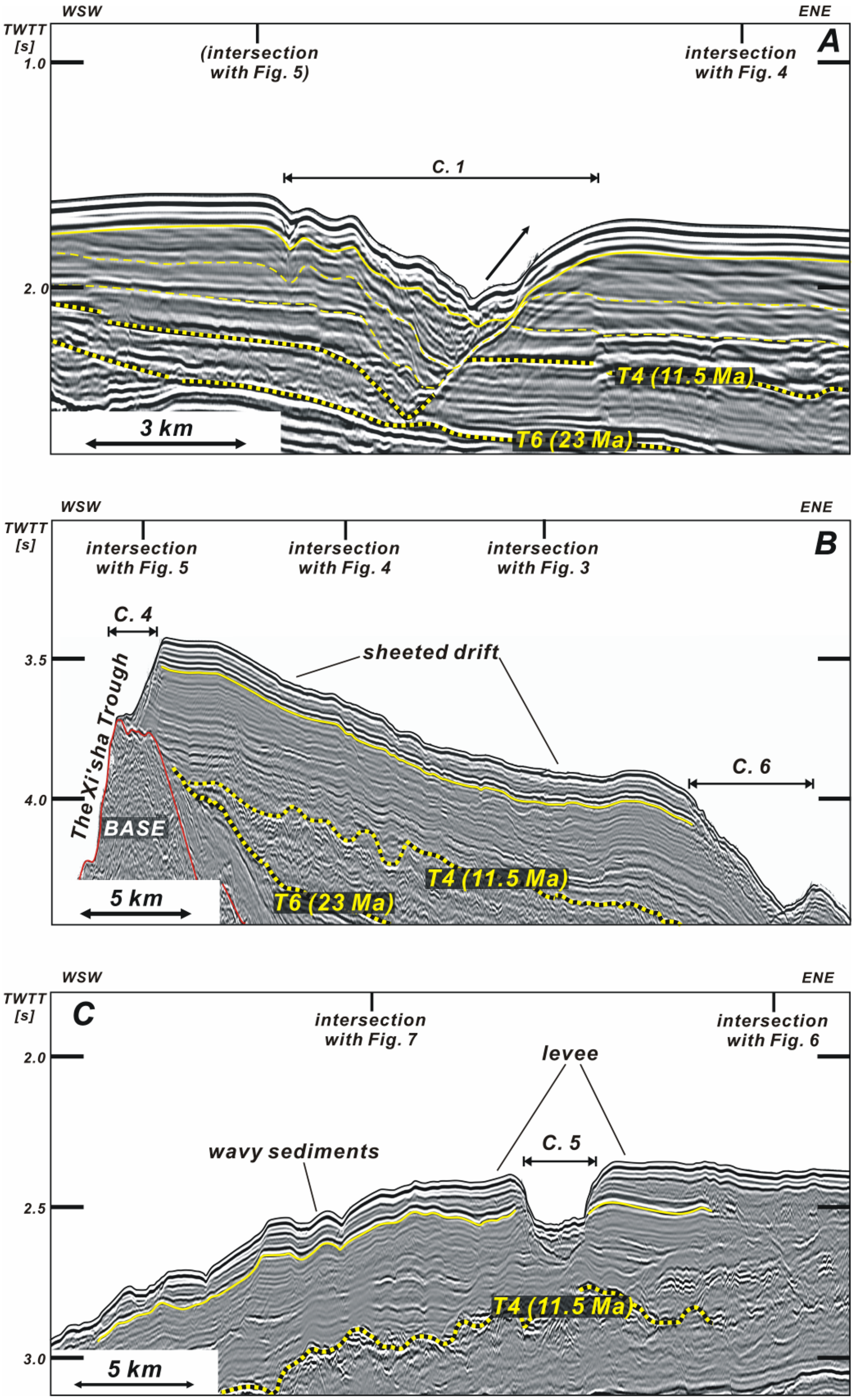
WSW
ENE
TWTT
[s]
1.0
(intersection
with Fig. 5)
intersection
with Fig. 4
A
C. 1
2. 0
T4 (11.5 Ma)
3 km
T6 (23 Ma)
WSW
ENE
TWTT
[s]
intersection
with Fig. 5
intersection
with Fig. 4
intersection
with Fig. 3
B
C. 4
3.5
sheeted drift
The Xi'sha Trough
4.0
BASE
C. 6
5 km
T4 (11.5 Ma)
T6 (23 Ma)
WSW
ENE
TWTT
[s]
C
intersection
with Fig. 7
intersection
with Fig. 6
2.0
levee
C. 5
wavy sediments
2.5
T4 (11.5 Ma)
3.0
5 km

FIG. 9

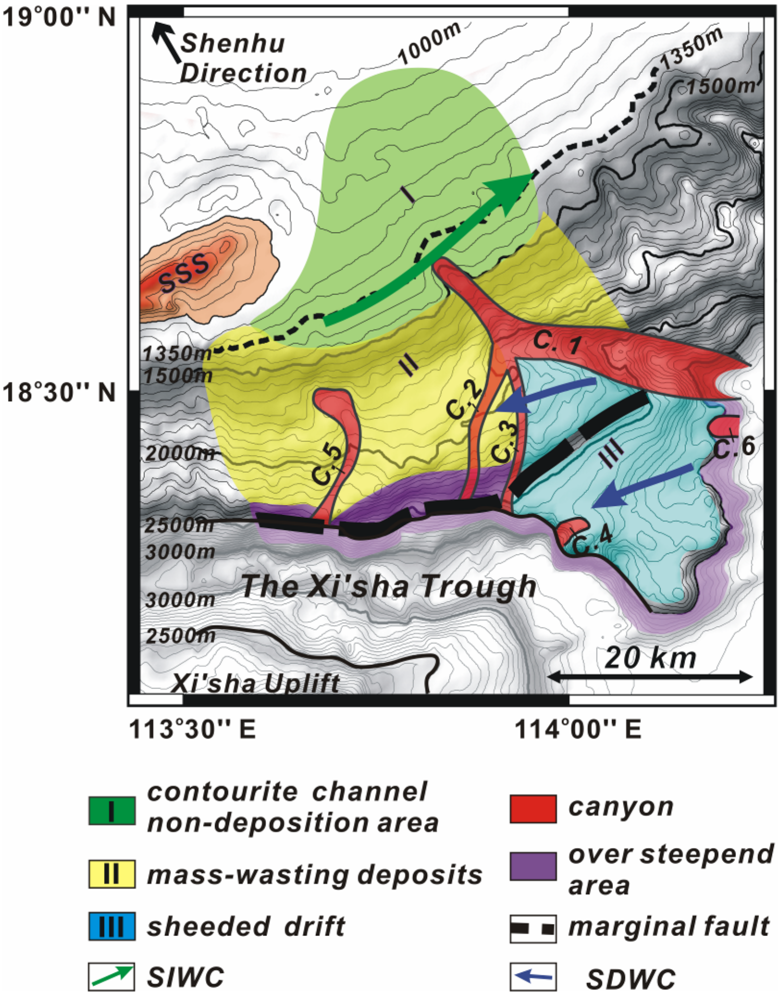

19°00'' N
18°30'' N
113°30'' E
114°00'' E
Shenhu Direction
1000m
1350m
1500m
2000m
2500m
3000m
SSS
I
II
III
C. 1
C.2
C.3
C.4
C.5
C.6
The Xi'sha Trough
Xi'sha Uplift
20 km
contourite channel non-deposition area
mass-wasting deposits
sheeded drift
SIWC
canyon
over steepend area
marginal fault
SDWC

FIG. 10

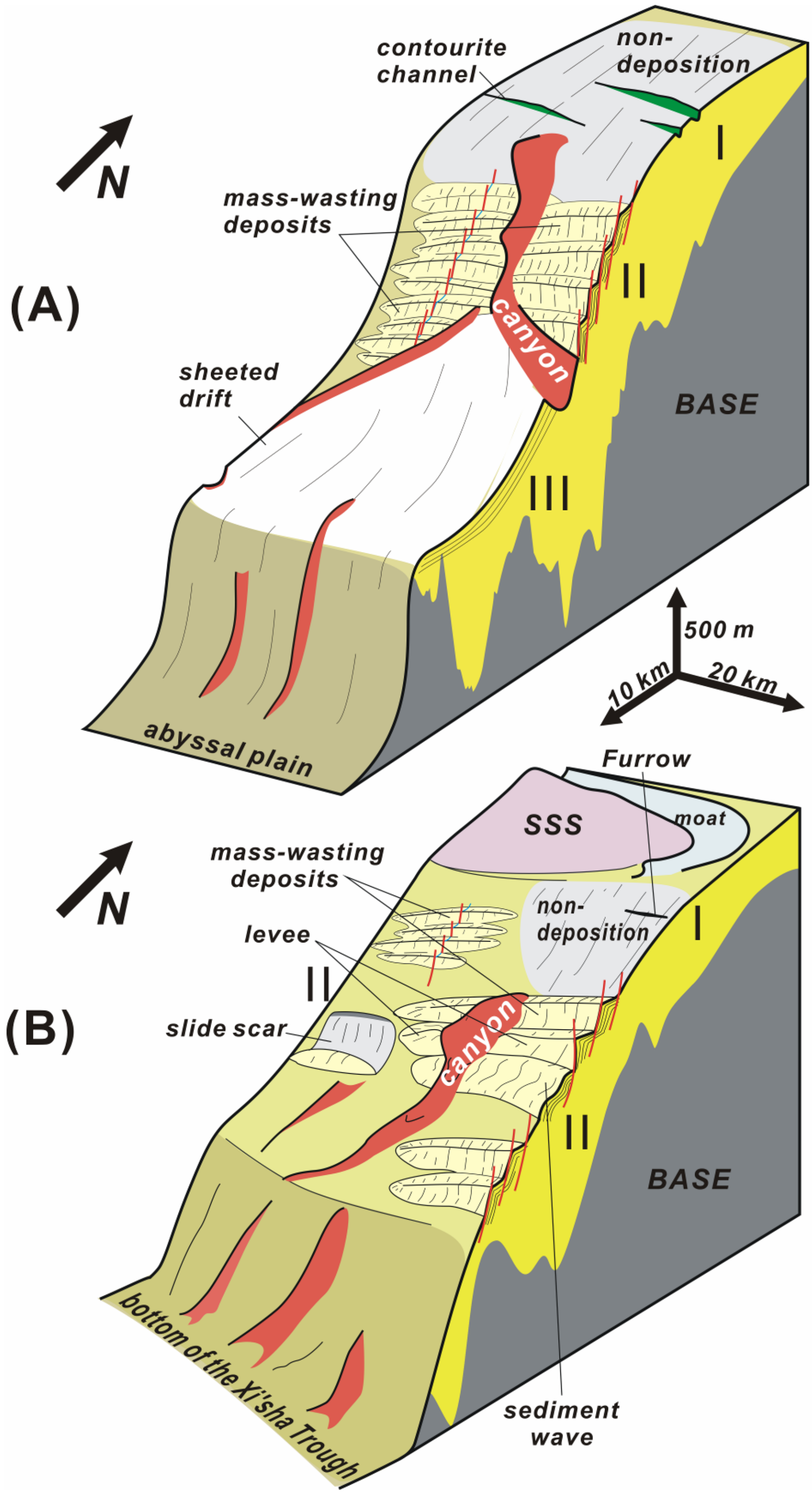

(A)
N
contourite channel
non-deposition
I
mass-wasting deposits
II
canyon
sheeted drift
BASE
III
500 m
10 km
20 km
abyssal plain
(B)
N
Furrow
SSS
moat
mass-wasting deposits
non-deposition
I
levee
II
slide scar
canyon
II
BASE
bottom of the Xi'sha Trough
sediment wave